Accepted Manuscript

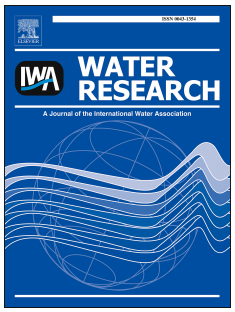

Petroleomic analysis of the treatment of naphthenic organics in oil sands process-affected water with buoyant photocatalysts

Tim Leshuk, Kerry M. Peru, Diogo de Oliveira Livera, Austin Tripp, Patrick Bardo, John V. Headley, Frank Gu

PII: S0043-1354(18)30373-7

DOI: 10.1016/j.watres.2018.05.011

Reference: WR 13776

To appear in: *Water Research*

Received Date: 4 February 2018

Revised Date: 8 May 2018

Accepted Date: 9 May 2018

Please cite this article as: Leshuk, T., Peru, K.M., de Oliveira Livera, D., Tripp, A., Bardo, P., Headley, J.V., Gu, F., Petroleomic analysis of the treatment of naphthenic organics in oil sands process-affected water with buoyant photocatalysts, *Water Research* (2018), doi: 10.1016/j.watres.2018.05.011.

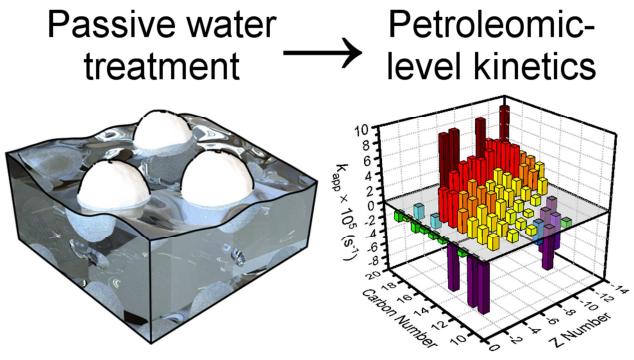

Petroleomic analysis of the treatment of naphthenic organics in oil sands process-affected water with buoyant photocatalysts

Tim Leshuk,[a,b] Kerry M. Peru,[c] Diogo de Oliveira Livera,[a,b] Austin Tripp,[a,b] Patrick Bardo,[a,b] John V. Headley,[c] Frank Gu*[,a,b]

[a]Department of Chemical Engineering and [b]Waterloo Institute for Nanotechnology, University of Waterloo, Waterloo, Ontario, Canada N2L 3G1. [c]Water Science and Technology Directorate, Environment & Climate Change Canada, Saskatoon, Saskatchewan, Canada S7N 3H5.

*Corresponding author. Phone: +1 519 888 4567 ext. 38605 Fax: +1 519 888 4347 Email: frank.gu@uwaterloo.ca

Abstract

The persistence of toxicity associated with the soluble naphthenic organic compounds (NOCs) of oil sands process-affected water (OSPW) implies that a treatment solution may be necessary to enable safe return of this water to the environment. Due to recent advances in high-resolution mass spectrometry

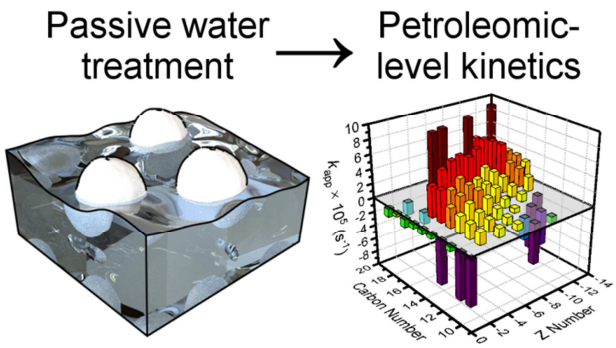

(HRMS), the majority of the toxicity of OSPW is currently understood to derive from a subset of toxic classes, comprising only a minority of the total NOCs. Herein, oxidative treatment of OSPW with buoyant photocatalysts was evaluated under a petroleomics paradigm: chemical changes across acid-, base- and neutral-extractable organic fractions were tracked throughout the treatment with both positive and negative ion mode electrospray ionization (ESI) Orbitrap MS. Elimination of detected OS^+ and NO^+ classes of concern in the earliest stages of the treatment, along with preferential degradation of high carbon-numbered O_2^- acids, suggest that photocatalysis may detoxify OSPW with higher efficiency than previously thought. Application of petroleomic level analysis offers unprecedented insights into the treatment of petroleum impacted water, allowing reaction trends to be followed across multiple fractions and thousands of compounds simultaneously.

Keywords

naphthenic acid; titanium dioxide; floating; passive; positive ion; advanced oxidation process

Highlights

- Oil sands process-affected water (OSPW) is impacted by naphthenic organic compounds (NOCs)
- Majority of OSPW toxicity attributed to only a subset of NOC classes
- Passive treatment of OSPW demonstrated with buoyant photocatalyts
- First time petroleomics used to study treatment kinetics across NOC fractions
- Preferential degradation of priority O_2^-, OS^+ and NO^+ NOC classes of concern

List of Acronyms

AEO	Acid extractable organics
AOP	Advanced oxidation process
BEO	Base extractable organics
BPCs	Buoyant photocatalysts
ESI	Electrospray ionization
ESI(-) MS	Negative ion mode ESI mass spectrometry
ESI(+) MS	Positive ion mode ESI mass spectrometry
HGMs	Hollow glass microspheres
HRMS	High resolution mass spectrometry
NAs	Naphthenic acids, of the general formula $C_cH_{2c+Z}O_2$
NEO	Neutral extractable organics
NOCOCs	Naphthenic organic classes of concern
NOCs	Naphthenic organic compounds, of general formula $C_cH_{2c+Z}N_nO_oS_s$
OSPW	Oil sands process-affected water
PC	Photocatalysis
WET	Whole effluent toxicity

Introduction

The Clark process used for extraction of bitumen in Canada's oil sands generates large volumes of water as a by-product, referred to as oil sands process-affected water (OSPW), which is stored on site in tailings ponds for water recycling. The oil sands mining companies are

obligated to eventually return this water to the environment (Martin, 2015; *Lower Athabasca Region - Tailings Management Framework for the Mineable Athabasca Oil Sands*, 2015, *Directive 085: Fluid Tailings Management for Oil Sands Mining Projects*, 2017). Currently, however, they are operating on a zero-discharge policy, due in part to the water's toxicity, which is primarily attributed to dissolved bitumen-derived organics.(Verbeek et al., 1994; Hughes et al., 2017b; Brown and Ulrich, 2015; McQueen et al., 2017b) Fractions of these organics are highly persistent,(Han et al., 2009; Quagraine et al., 2005) and remain potently toxic even after decades of aging.(Marentette et al., 2015) Thus treatment of OSPW may be required to enable safe discharge, and the industry is currently exploring passive remediation solutions.("COSIA Challenge #0014: Passive Organics Treatment Technology," 2015)

In the past, the organic constituents of OSPW were thought to simply comprise naphthenic acids (NAs), of the classical formula $C_cH_{2c+Z}O_2$, where *Z* indicates hydrogen deficiency from rings or double bonds.(Clemente and Fedorak, 2005) However, with the advance of analytical capabilities such as high-resolution mass spectrometry (HRMS), far more complexity has been revealed (Barrow et al., 2015, 2010; Grewer et al., 2010). OSPW is now understood to contain not only these conventional NAs, but also oxidized and heteroatomic classes,(Barrow et al., 2014) and non-acid neutral and basic species,(Barrow et al., 2016) referred to collectively herein as naphthenic organic compounds (NOCs, of general formula $C_cH_{2c+Z}N_nO_oS_s$). While classic NAs are known toxicants,(Hughes et al., 2017b) recent effects-directed analyses have also shown these base-neutral organics contribute significantly to the toxicity of OSPW,(Morandi et al., 2017, 2015) and may also be implicated in its endocrine disruptive effects.(Rowland et al., 2011; Pereira et al., 2013) With the petroleomic level insights afforded

by such rich HRMS datasets,(Marshall and Rodgers, 2008; McKenna et al., 2013) it has even been proposed recently that the whole effluent toxicity (WET) of OSPW may be predictable simply through mass spectral analysis.(Morandi et al., 2016)

While many of these analytical advances have been driven by the goals of environmental forensics,(Frank et al., 2014; Headley et al., 2013, 2011; C. Sun et al., 2017) it is important for water treatment technologies to keep pace with the scientific progress and be evaluated with the same analytical rigor, to provide validated remediation tools for emergent environmental priorities. In terms of technologies studied for OSPW treatment, solar photocatalysis (PC) has been shown to be particularly effective at eliminating NAs,(Headley et al., 2009; Leshuk et al., 2016b, 2016a; Liu et al., 2016; McQueen et al., 2017a) and may be the only advanced oxidative process (AOP) with the potential for deployment in passive treatment systems, given the vast sunlight-exposed surface area of tailings ponds. However, the capacity of PC to treat base-neutral fraction NOCs has not been previously studied.

The objective of this work was to evaluate the performance of buoyant photocatalysts (BPCs) to degrade NOCs in OSPW, while tracking chemical changes across acid-, base- and neutral-extractable organic fractions with HRMS. Through combining pH fractionation with both positive and negative ion mode MS, we aimed to gain an unprecedented petroleomic perspective of the PC treatment of OSPW, by following molecular transformations across thousands of species simultaneously. While the photochemistry of petroleum has long been studied with low mass resolution techniques (Payne and Phillips, 1985; Shankar et al., 2015; Ziolli and Jardim, 2003; D'Auria et al., 2009; García-Martínez et al., 2006), and recently with FT-ICR MS (Griffiths et al., 2014), this is the first time PC, as a water treatment method, has been

87 studied through the lens of petroleomics, not only capturing a more holistic picture of the
88 chemical changes occurring during NOC oxidation, but also exposing new insights into
89 treatment of emerging naphthenic organic classes of concern (NOCOCs). As not all OSPW
90 organics are equally toxic,(Hughes et al., 2017b; Morandi et al., 2015) tracking elimination of
91 specific NOCOCs in a complex mixture, rather than simply measuring reduction of bulk organic
92 metrics, may represent a new standard for evaluating treatment solutions for petroleum
93 impacted waters.

94 Experimental

95 Materials

96 OSPW was provided by an industrial producer operating in the Athabasca oil sands, and stored
97 in sealed polyethylene containers in the dark at 4 °C for 16 weeks prior to testing. The OSPW
98 was homogenized by stirring before each use, and then centrifuged (14,000 xg) or filtered
99 (Whatman 934-AH glass fiber filter) to remove suspended solids, depending on test volume
100 requirements.

101 A commercial mixture of naphthenic acids (technical grade, carbon numbers 6 – 20, *Z* numbers
102 0 to -4, as characterized by Damasceno et al. (Damasceno et al., 2014)), dichloromethane (DCM,
103 ≥99.9%, HPLC grade), NH_4OH (28-30%, ACS grade), HNO_3 (70%, ACS grade), HCl (37%, ACS
104 grade) tetraethylorthosilicate (TEOS, 98%) and Pluronic F127 were purchased from Sigma-
105 Aldrich and used as received. Sulfuric acid (95-98%, ACS grade, Fisher), ethanol (EtOH, ACS
106 grade) and TiO_2 nanoparticles (Aeroxide P25, ~10-50 nm particle diameter, 55 $m^2 g^{-1}$ surface
107 area, Acros) were used as received. Hollow glass microspheres (HGMs, 3M iM30k, soda-lime-

borosilicate glass, ~10-30 μm diameter, 0.6 g/cm^3 density) were washed by 1 mol/L HNO_3 or H_2SO_4 before use (at 125 g/L microspheres), 3-5 times with deionized (DI) water by flotation, then dried at 120 °C in air.

Buoyant photocatalyst (BPC) synthesis

A silica sol-gel solution was prepared as previously.(Allain et al., 2007) Briefly, an acidic ethanolic TEOS solution of molar ratio TEOS:EtOH:H_2O:HCl = 1:4:10:0.01 was hydrolysed at 60 °C for 1 h, and then cooled to room temperature before use. TiO_2 nanoparticles and Pluronic F127 were then dispersed into DI H_2O by probe sonication, after which silica sol-gel solution and 1 mol/L HNO_3 were added to achieve a molar ratio of Ti:Si:F127 = 1:1:0.01, 0.1 mol/L HNO_3, and 25 g/L TiO_2. This TiO_2 suspension was then added to HGM powder at a 2:1 volume:mass ratio, and dried at room temperature for ≥24 h. The dried cake was then crushed to a powder, calcined for 6 h at 400 °C in air to remove the polymeric templates, and then washed with DI H_2O by flotation and dried. Particle morphology was analyzed by SEM (Zeiss Merlin FESEM).

Photocatalytic experiments

Photocatalytic experiments were performed in a custom photoreactor enclosure, consisting of an array of UVA fluorescent bulbs (Philips F20T12/BL, peak emission ~350 nm) suspended above the samples.(Leshuk et al., 2016a) The UV intensity was measured to be ~36 W/m^2 with a UVA/B light meter (Sper Scientific, NIST certified calibration), which is similar to the UV content of the solar spectrum (46.6 W/m^2, ASTM G173-03 global tilt). Our previous work demonstrated equivalent photocatalytic treatment rate of OSPW in this photoreactor as under natural sunlight (Leshuk et al., 2016b, 2016a).

For the principal treatment study (Figure 2-Figure 5), BPCs were added at 300 g/m^2 (≈13.8 g/m^2 TiO_2) to 1 L of OSPW in a borosilicate glass beaker (11 cm I.D., sides wrapped with Al foil), which was sealed with UV-transparent polyethylene film. Beakers were equilibrated in the dark for 1 h, then placed in the photoreactor and exposed to UV light while stirring at 300 rpm (PTFE coated stir bar, 3.81 × 0.95 cm l × d), with periodically sampling (1 mL for UV_{220}) and addition of DI H_2O (Millipore, ≥15 MΩ·cm) to correct for evaporation losses. Beaker temperatures equilibrated at ~23 °C during the exposure. Following the UV treatment, the OSPW mixture was vacuum filtered (Whatman 934-AH glass fiber filter) to remove BPC particles, and the filtrate retained for analysis (stored at 4 °C in the dark for <24 h before extraction).

Preliminary experiments on the effect of depth, mixing intensity, catalyst concentration and recyclability (Figure S2-Figure S5) were conducted in 500 mL PTFE beakers (7.2 cm I.D.) at a UV intensity of ~26 W/m^2, with typical levels (i.e., held constant when varying the other factors) of 125 g/m^2 (≈5.8 g/m^2 TiO_2) for BPC coverage, 300 mL OSPW, and 130 rpm stirring, with kinetics measured by UV_{220}. OSPW UV absorbance has been previously shown to correlate with NOC concentration (Mohamed et al., 2008), and 220 nm was monitored in this work as it provided the highest signal-to-noise ratio. Depth was varied by testing different volumes of OSPW in the same beakers. For the recyclability study, between UV exposures BPCs were separated by flotation, rinsed thrice with DI H_2O, then added to fresh OSPW for another treatment cycle.

Liquid-liquid extraction (pH fractionation)

For organics extraction, 200 mL OSPW was adjusted with H_2SO_4 to either pH 2.0 (to ensure protonation of carboxylic acids) for acid-extractable organics (AEO), or pH 7.0 ± 0.1 for neutral-

extractable organics (NEO), or with NH_4OH to pH 10.5 for base-extractable organics (BEO), then extracted with 100 mL DCM (40, 40, and 20 mL sequentially), after which the extract was dried under N_2. NEO and BEO were collected to investigate NOCs that may not be extractable under acidic conditions thereby not appear in typical AEO analyses.

For total extractable organics (total EO), 400 mL OSPW was first adjusted to pH 10.5 with NH_4OH and extracted with 100 mL DCM, then to pH 7.0 ± 0.1 with H_2SO_4 and again extracted with 100 mL DCM, then to pH 2.0 with H_2SO_4 and again extracted with 100 mL DCM, after which the extracts were combined and dried under N_2. This extract was used to gravimetrically prepare a standard curve for UV_{220} (Figure S1), and from the absorbance of OSPW prior to extraction, extraction efficiency was determined to be 49.1%, based on extract mass.

Analysis

AEO_{FTIR} was measured by Fourier transform infrared spectroscopy (FTIR) according to the standard method(Holowenko et al., 2001; Jivraj et al., 1995) with minor modifications (*viz.*, the acidified samples were extracted thrice with DCM in a 1:12.5 solvent:sample volumetric ratio, with 80 ± 4% total recovery), using the commercial NA mixture to prepare the calibration curve. UV absorbance at 220 nm (UV_{220}) was measured with a spectrophotometer (BioTek Epoch).(Mohamed et al., 2008) Chemical oxygen demand (COD) was measured with a test kit (Hach, APHA 5220D). Total organic carbon (TOC, APHA 5310B), biochemical oxygen demand (BOD, APHA 5210B), anion concentration by ion chromatography (EPA 300.1), alkalinity (as $CaCO_3$, EPA 310.2), and dissolved metals by inductively coupled plasma mass spectrometry (ICPMS, APHA 3030B/6020A) were measured according to standard methods by ALS

171 Environmental (Waterloo, ON, Canada), a laboratory accredited by the Canadian Association for
172 Laboratory Accreditation (CALA) according to international standards (ISO 17025).

173 HRMS Analysis

174 Dried extracts from the pH fractionation liquid-liquid extractions as described above (AEO, NEO
175 and BEO) were each individually re-dissolved in DCM. Each DCM solution was split into two
176 equal portions (with the exception of the NEO extract, as no pH modifier was used for re-
177 dissolution for either ion mode) and again brought to dryness under a gentle stream of N_2. The
178 split dried extracts were then re-dissolved in a solvent system based on the corresponding
179 HRMS analysis listed below. For the AEO extract: one dried extract was re-dissolved in 50:50
180 acetonitrile (ACN):water with 0.1% NH_4OH, and run in negative ion mode with 50:50 ACN:H_2O
181 with 0.1% NH_4OH as the LC eluent; the second extract was re-dissolved in 50:50 ACN:H_2O with
182 no pH modifier, and run in positive ion mode with 0.1% formic acid (HCOOH) as the LC eluent.
183 For the BEO extract: one dried extract was re-dissolved in 50:50 ACN:H_2O with 0.1% HCOOH,
184 and run in positive ion mode with 50:50 ACN:H_2O with 0.1% HCOOH as the mobile phase; the
185 second extract was re-dissolved in 50:50 ACN:H_2O with no pH modifier, and run in negative ion
186 mode with 0.1% NH_4OH as the mobile phase. For the NEO extract: the dried extract was re-
187 dissolved in in 50:50 ACN:H_2O with no pH modifier, and run in positive ion with 50:50 ACN:H_2O
188 with 0.1% ACN:H_2O as the mobile phase, and again in negative ion mode with 50:50 ACN:H_2O
189 with 0.1% NH_4OH as the mobile phase.

190 Mass spectrometry analysis was performed using an LTQ Orbitrap Elite (Thermo Fisher
191 Scientific, San Jose, CA) operating in full scan in negative and positive ion mode. Mass
192 resolution was set to 240,000 with an *m*/*z* scan range of 100-600. For negative ion mode the ESI

source was operated as follows: sheath gas flow rate 10 (arbitrary units), spray voltage 2.90 kV, auxiliary gas flow rate 5 (arbitrary units), S lens RF level 67 %, heater temperature 50 ^{o}C, and capillary temperature 275 ^{o}C. For positive ion mode the ESI source was operated as follows: sheath gas flow rate 10 (arbitrary units), spray voltage 3.00 kV, auxiliary gas flow rate 5 (arbitrary units), S lens RF level 63 %, heater temperature 50 ^{o}C, and capillary temperature 275 ^{o}C. As per Composer data analysis, the mass accuracy was < 2 ppm error for all mass assignments.

For negative ion analysis, the mobile phase solvent used was 50:50 ACN:H_2O containing 0.1 % NH_4OH, while positive ion analysis used 50:50 ACN:H_2O containing 0.1 % HCOOH. Given that the same mobile phase was used for all samples in each ionization mode, class ionization efficiency was assumed to be independent of extraction pH when comparing between the different pH fractions. A flow rate of 200 µL min^{-1} was used for both, delivered by an Accela 1250 solvent pump (Thermo Fisher Scientific, San Jose, CA). A volume of 5 µL was injected into the mobile phase stream using a Thermo PAL-HTC Accela autosampler (Thermo Fisher Scientific, San Jose, CA). Quantitation was performed using linear regression obtained from a 5 point external calibration.(Hughes et al., 2017b)

The software used for instrument control/data acquisition and molecular analysis was Xcalibur version 2.1 (Thermo Fisher Scientific, San Jose, CA) and Composer version 1.5.2 (Sierra Analytics, Inc., Modesto, CA), respectively. Pseudo-first order rate constants were fit to the $O_2^{\pm}$ class data based on initial trends of when congeners were first detected in the reaction (since some congeners displayed complex trends of intensity increasing initially, but decreasing later in the treatment). For comparisons between the different pH fractions, it was assumed that the

ionization efficiency of a given class was independent of extraction pH, given that pH of the mobile phase was the same.

Results and Discussion

Buoyant photocatalyst (BPC) design

Previous OSPW treatment studies have evaluated nanoparticle photocatalysts dispersed as slurries in the OSPW,(Headley et al., 2009; Leshuk et al., 2016b; Mishra et al., 2010) which, while useful as performance benchmarks, are impractical for passive deployment due to the requirement for vigorous mixing to keep the particles suspended, the challenge of catalyst recovery, and concern of environmental release of nanoparticles. Since solar PC is driven by sunlight absorption at the water surface, we hypothesized that by immobilization on buoyant supports, photocatalysts could remain suspended in the illuminated zone without the requirement for mixing, while enabling simple catalyst retention and separation following treatment. Such a design should also result in more efficient materials utilization, since photocatalyst particles are not dispersed in the dark zone below the water surface where they are unreactive and result in catalyst oversupply, in contrast to slurry dispersions. BPCs have been successfully demonstrated for treatment of simulated oil spills and dissolved organics.(Berry and Mueller, 1994; Magalhães and Lago, 2009; Nair et al., 1993) Given their proven potential, we thus sought to demonstrate BPCs for OSPW treatment.

BPC composite particles were synthesized by coating TiO_2 nanoparticles on hollow glass microspheres, using mesoporous silica as a binder (Figure 1). Binding nanoparticles within composite materials is a successful strategy to control the environmental release of free

236 nanoparticles (Froggett et al., 2014; Ging et al., 2014). Purely inorganic materials were selected
237 for the composites to resist photocatalytic attack,(Fabiyi and Skelton, 2000; Shang et al., 2003;
238 Singh et al., 2013) and a porous silica binder was used to enhance nanoparticle adhesion to the
239 microsphere support,(Qiu and Zheng, 2007) while still allowing access of solution to the catalyst
240 via mesopores.(Allain et al., 2007) The synthesized BPC material was hydrophilic, and floated at
241 the surface of water as a frothy film (Figure 1d&e).

242

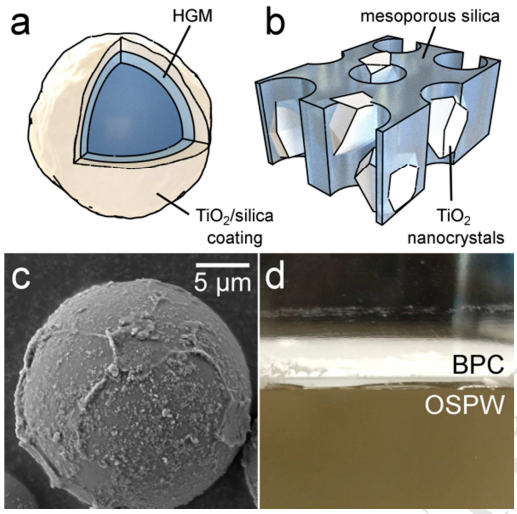

243

244 **Figure 1.** Schematic drawings of (a) BPC composite structure and (b) TiO_2 nanoparticles
245 immobilized in mesoporous silica, (c) SEM image of a BPC composite particle, and (d)
246 photograph of a BPC film floating on OSPW, from a side view.

247 The PC performance of the BPCs were evaluated in OSPW. Treatment rate diminished as a
248 function of water depth (Figure S2), consistent with a surface driven reaction, where >99% of
249 UV light was absorbed within the top cm of OSPW in previous photocatalytic experiments
250 (Leshuk et al., 2016b). Notably, the apparent rate of the BPCs (~4.3×10^{-6} s^{-1}) was similar to that

of a TiO_2 nanoparticle slurry (P25) at low concentrations (<5 g/m^2 TiO_2, Figure S3) and gentle mixing conditions (Re < 1000, Figure S4), although the TiO_2 slurry was more efficient under vigorous mixing (Re > 1000) and at higher concentrations (>5 g/m^2 TiO_2). The BPCs were also found to maintain their performance over 10 batch treatment cycles (Figure S5). Thus when operating under non-turbulent flow regimes, BPCs match the performance of TiO_2 slurries, while enabling easier retention and recycling than free nanoparticle dispersions (Chong et al., 2010; Malato et al., 2009).

Overall treatment kinetics

Following these preliminary experiments, the transformation of NOCs during the photocatalytic process was thoroughly investigated. The initial organics concentrations in the OSPW were measured by several methods (Table 1; inorganic parameters given in Table S1; FTIR and MS spectra given in Figure S6 and Figure S7-Figure S36, respectively). A relatively low BOD number compared to the other metrics is typical for OSPW, and indicates the recalcitrance of the NOCs to biodegradation (Leshuk et al., 2016b). The difference of AEO concentrations measured by FTIR and MS is likely due to the use of a commercial NA mixture (with low average molecular weight) as the calibration standard for the FTIR method.(Hughes et al., 2017a) The most organics (by ESI(-) MS) were extracted at neutral pH with 113.5 mg/L NEO, ~42% more than the acidic extract, and ~19-fold more than the basic extract. Previous studies have similarly measured reduced extraction of negative ion species at high pH.(Huang et al., 2016; Klamerth et al., 2015) This comparison assumes class response factors are independent of extraction pH for a given ionization mode. The high NEO:AEO ratio may be evidence of polar non-acids partitioning to the neutral fraction.

Table 1. Measures of dissolved organics in raw OSPW.

Parameter	Concentration (mg/L)
AEO_{FTIR}	40.9 ± 2.4
AEO_{MS}[a]	79.9
NEO_{MS}[a]	113.5
BEO_{MS}[a]	6.0
Total EO (UV_{220})	78.9 ± 1.9
TOC	54
COD	153
BOD	3.0

[a] Concentrations calculated only from negative ion MS data, assuming an extraction efficiency of 49.1%.

During the photocatalytic reaction, FTIR was found to be a good surrogate measure for MS kinetics. The apparent pseudo-first order rate constant (k_{app}) of AEO_{FTIR} removal, $9.2 \pm 0.4 \times 10^{-6}$ s^{-1}, matched closely to that of AEO_{MS} removal, $11.4 \pm 0.4 \times 10^{-6}$ s^{-1} (Figure 2a).(Hughes et al., 2017a; Islam et al., 2014) The NEO and BEO were eliminated significantly more quickly than the AEO, with $k_{app} = 25.1 \pm 0.7 \times 10^{-6}$ s^{-1} and $14.9 \pm 1.3 \times 10^{-6}$ s^{-1}, respectively. This may be reasonable on the basis that ring-opening photocatalytic reactions form carboxylic acid groups,(Bui et al., 2011; Grabowska et al., 2012; Pichat, 1997; Soana et al., 2000) which would

285 be expected to lead to accumulation of originally base-neutral species in the AEO fraction over
286 the course of the treatment (Figure 2b). Continuation of photocatalytic exposure resulted in
287 final organics mineralization (reduced COD and TOC, Figure 2a), in contrast to weaker oxidation
288 processes such as ozonation, which have been shown to leave a toxic organic residual in OSPW
289 even after high O_3 doses (>30 mg/L).(Klamerth et al., 2015; Meshref et al., 2017; Scott et al.,
290 2008) Effective photocatalytic NOC mineralization may be due to the high oxidation potential of
291 TiO_2 valence band holes (~3.0 V vs. SHE),(Nosaka and Nosaka, 2013) or the involvement of
292 superoxide radicals, as hypothesized previously (de Oliveira Livera et al., 2018; Leshuk et al.,
293 2016b). Faster elimination of extractable organics compared to UV_{220}, COD, and TOC, may be
294 due to a process of photocatalytic oxidation initially increasing the polarity of the organics to
295 the point where they are no longer extractable by DCM at any pH, after which they are steadily
296 mineralized. AEO_{FTIR} was only reduced by 11% (4.6 mg/L) in a catalyst-free OSPW control
297 exposed to a UV fluence of 27.8 MJ m^{-2}, similar to previous observations of minimal photolytic
298 elimination in the absence of a catalyst (Leshuk et al., 2016b).

299

300

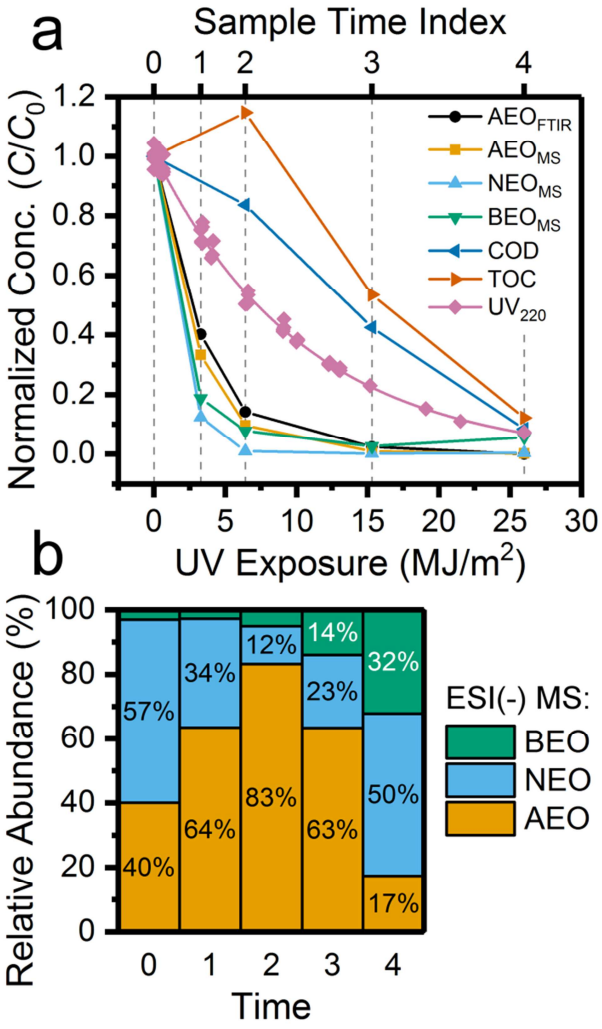

Figure 2. (a) Photocatalytic treatment kinetics by various organics measures. Samples taken throughout the treatment were labelled by a sequential Time Index. (b) Ratios of AEO, NEO, and BEO negative ion concentrations throughout the photocatalytic reaction, with time indices corresponding to those labeled in (a).

Heteroatomic class transformations

Recently, heteroatomic and positive ion classes have been implicated in the toxicity of OSPW,(Alharbi et al., 2016; Morandi et al., 2017, 2015) therefore it is important to understand

their transformations during PC. In terms of initial speciation of negative ions, the neutral and basic fractions were dominated by O_2^- (classic NAs), while the AEO additionally contained minority O_3^-, O_4^- and O_3S^- classes (Figure S37). A high O_2^- ratio (relative to O_o^- classes with *o* >2) may indicate a relatively fresh OSPW sample, as *o* increases with environmental aging.(Han et al., 2009) As observed previously,(Barrow et al., 2010) a greater diversity of heteroatomic classes were detected in positive ion mode (Figure S38). The BEO was primarily characterized by OS^+ (28%), O_8^+ (23%) and NO_8^+ (26%) classes, the AEO by SO_3^+ (59%), and the NEO by OS^+ (29%) and O_3S^+ (32%), along with minor NO^+ (3.8%), O_2^+ (7.7%), O_3^+ (4.2%), O_8^+ (5.8%) and O_2S^+ (3.6%).

In terms of environmental implications, O_2^- has been repeatedly confirmed as one of the most acutely toxic negative ion classes, with a narcotic mechanism arising from the NAs' surfactant properties (Hughes et al., 2017b; Morandi et al., 2015; Roberts and Costello, 2003; Yue et al., 2015b). Higher oxygen numbered species are less acutely toxic.(Frank et al., 2009) O_3S^- may comprise sulfonic acids, and thus impart similar surfactant modes of toxicity.(Quesnel et al., 2015) O_o positive ions likely contain hydroxyl or ketone groups, and may be implicated in the endocrine disrupting effects of OSPW.(Pereira et al., 2013; Rowland et al., 2011; Yue et al., 2015a) The O_3S^+ class is thought to comprise thiophenic hydroxylated aldehydes,(Rowland et al., 2014; J. Sun et al., 2017) and has previously been found in non-toxic NOC fractions.(Morandi et al., 2017, 2015) The O_2^-, O^+ and OS^+ classes have among the highest measured membrane partitioning ratios, with potential to bioaccumulate.(Zhang et al., 2015, 2016) While typically measured at lower intensity than the O_2^- NAs, OS^+ and NO^+ species are also thought to be potent toxicants,(Morandi et al., 2016) with potential to inhibit membrane transport proteins

and damage DNA through oxidative stress.(Alharbi et al., 2016; Morandi et al., 2017; J. Sun et al., 2017)

During the photocatalytic treatment, both positive and negative ions of the heteroatomic O_oS_s family were initially preferentially degraded (Figure 3), such that the class distributions shifted to almost exclusively O_o at intermediate time points (Figure S39). The relative increase in O_o^+ intensity observed in all extracts from the first treated sample (3.3 MJ/m^2 UV exposure) could be attributed to the appearance of oxidized intermediates. These changes in relative composition of heteroatomic classes, especially in the positive ion data (where the O_o fraction increases to ~90% from ~20% in the raw OSPW, Figure S39 ESI(+) trend), are much larger than observed previously following OSPW treatment with O_3, UV/H_2O_2 and Fe(VI) (relative changes of only ~20%) (Wang et al., 2016). This could potentially indicate a more selective oxidation mechanism for PC, in accordance with previous observations.(de Oliveira Livera et al., 2018; Leshuk et al., 2016b) In the final stages of the photocatalytic reaction, the abundance of $O_oS_s^-$ and $N_nO_o^+$/$N_nO_oS_s^+$ species relative to the $O_o^\pm$ increased in the AEO and NEO extracts, concurrently with the decreasing AEO fraction (Figure 2b). Under the assumption that ionization efficiency of a given class is similar across all samples investigated, it is hypothesized that while raw O_oS_s species are initially the most reactive NOCs, oxidized intermediates produced during the photocatalytic process are more reactive still, possibly due to preferential adsorption of acidic and catecholic moieties to TiO_2.(Dobson and McQuillan, 1999; Janković et al., 2009) If so, in the final stages of the treatment acidic O_o compounds could be preferentially degraded over base-neutral heteroatomics.

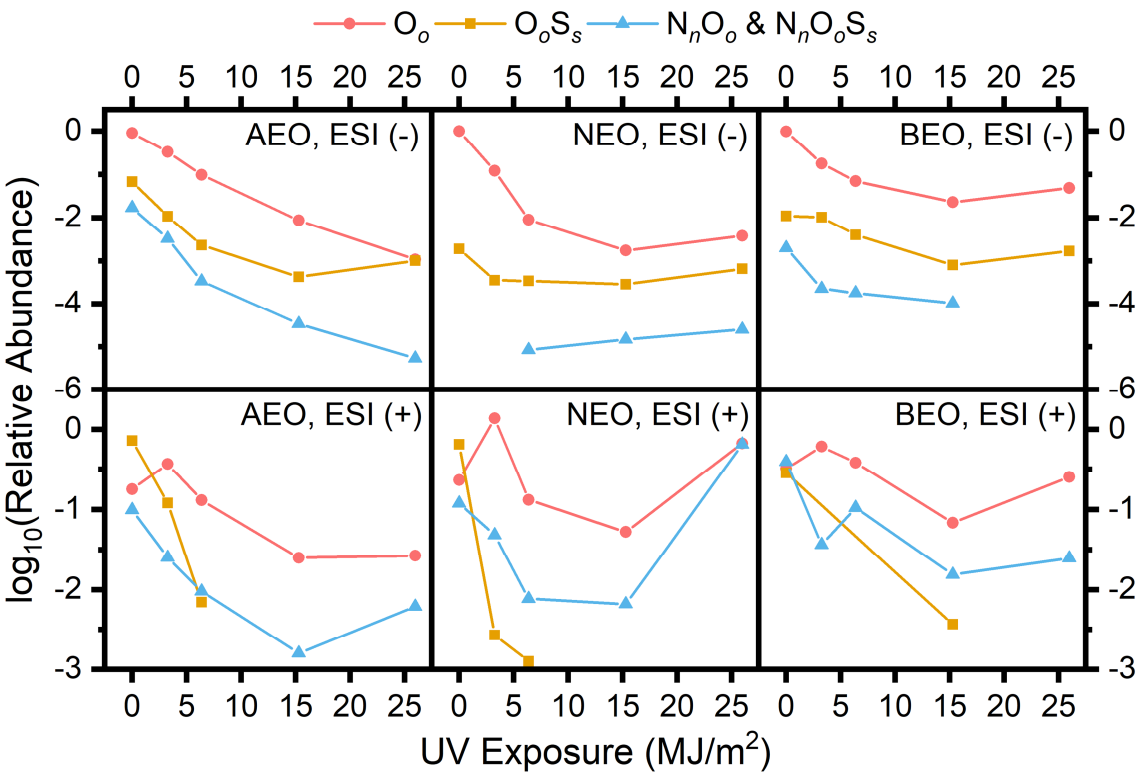

Figure 3. Relative abundance of heteroatomic families throughout the photocatalytic treatment. Relative abundance was normalized within each extract and ion mode to the total intensity measured in the initial raw OSPW.

Class oxidation trends

Oxygen number *o* > 2 has been generally shown to be inversely correlated with acute toxicity for OSPW NOCs, as the polarity of added oxygen functionalities counteracts the molecules' surfactant properties.(Frank et al., 2008; Yue et al., 2015b) While the intensity of the negative ions was significantly diminished by the first sampling time point (Figure 4), clear trends of increasing *o* with time were observed in all extracts for both O_o^- and O_oS^- classes (Figure S40,

363 normalized with respect to time point to highlight the oxidation trends). In the AEO, average *o*
364 increased from 2.5 in the raw OSPW to 4.3 by the third time point of photocatalytic exposure.
365 This is once again a stronger shift than was reported for OSPW AEO oxidation using other
366 AOPs,(Wang et al., 2016) although a similarly large increase in *o* has been observed previously
367 for photocatalytic OSPW AEO oxidation.(Leshuk et al., 2016b) Apparent deviation from this
368 trend in some extracts at the final two time points may simply be due to poor DCM extraction
369 efficiency of highly polar, heavily oxidized compounds in the final stages of the treatment.

370

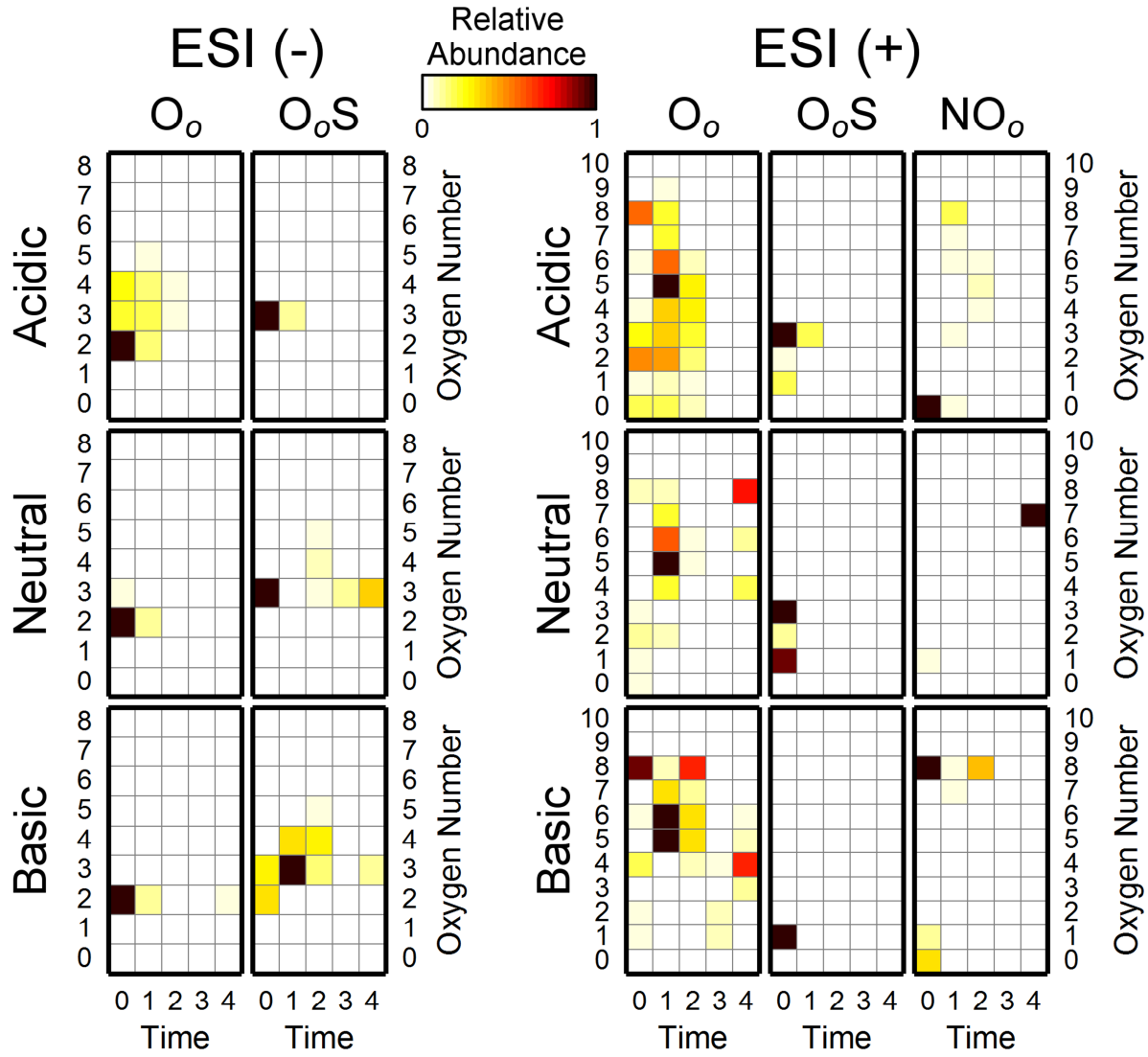

371

372 **Figure 4.** Trends in oxygen number (*o*) with time for different heteroatomic classes. Relative

373 abundance of species by oxygen number is presented normalized to the maximum intensity

374 measured within each class, where time indices correspond to those labelled in Figure 2a.

375

376 In positive ion mode, any trends in *o* with time were less clear: the broad distributions in O_o^+ in

377 the acidic and neutral extracts may be attributed to the appearance of hydroxylated oxidation

intermediates.(J. Sun et al., 2017) Indeed, the increased O_o^+ intensity at Time 1 is correlated with the reduction in O_o^- and O_oS^- abundance. Some single-class conclusions may also be drawn from the ESI(+) data: the OS^+ NOCOC was eliminated by the first time point in the BEO and NEO. Similarly, the NO^+ species in the neutral extract were eliminated by the first time point, along with the O_2^+ and O_3^+ classes.

Thus the presumed most toxic NOCOCs (O_2^-, OS^+ and NO^+)(Morandi et al., 2015; J. Sun et al., 2017) were rapidly transformed in the earliest stages of the treatment, when AEO_{FTIR} was still measured as 40%. This is promising for the practicality of photocatalytic OSPW treatment, as only a relatively short exposure may be needed to meet WET targets, rather than full organics mineralization. This is supported by our previous finding that OSPW toxicity towards *Vibrio fischeri* could be eliminated by solar PC prior to full organics mineralization,(Leshuk et al., 2016b) although more rigorous toxicity testing of PC treated OSPW is warranted.

Previous studies have shown that oxidized NOCs are more readily biodegradable.(Brown et al., 2013; Dong et al., 2015; Martin et al., 2010) Thus given the oxidation patterns observed herein, supplementation of PC with biodegradation may be another promising strategy to increase overall OSPW treatment efficiency, *e.g.*, by combination of solar PC with passive treatment wetlands.(Araña et al., 2008; Chow et al., 2017; McQueen et al., 2017a)

Carbon and Z number kinetics

In addition to following chemical transformations between classes, through HRMS it was also possible to investigate the molecular weight (carbon number *c*) and hydrogen deficiency (*Z* number) distribution within any single class throughout the photocatalytic treatment. We thus

399 fit a pseudo-first order rate constant to each $O_2^{\pm}$ species as a function *c* and *Z* (Figure 5). It
400 should be emphasized that the O_2^+ species are likely hydroxylated NOCs rather than NAs, but
401 they are still presented together with the O_2^- NAs for comparison of the relative reactivity of
402 positive and negative ions within the same treatment. Furthermore, since very few O_2^+
403 compounds were detected in the initial BEO (Figure S38), the data for Figure 5f is sparse.

404

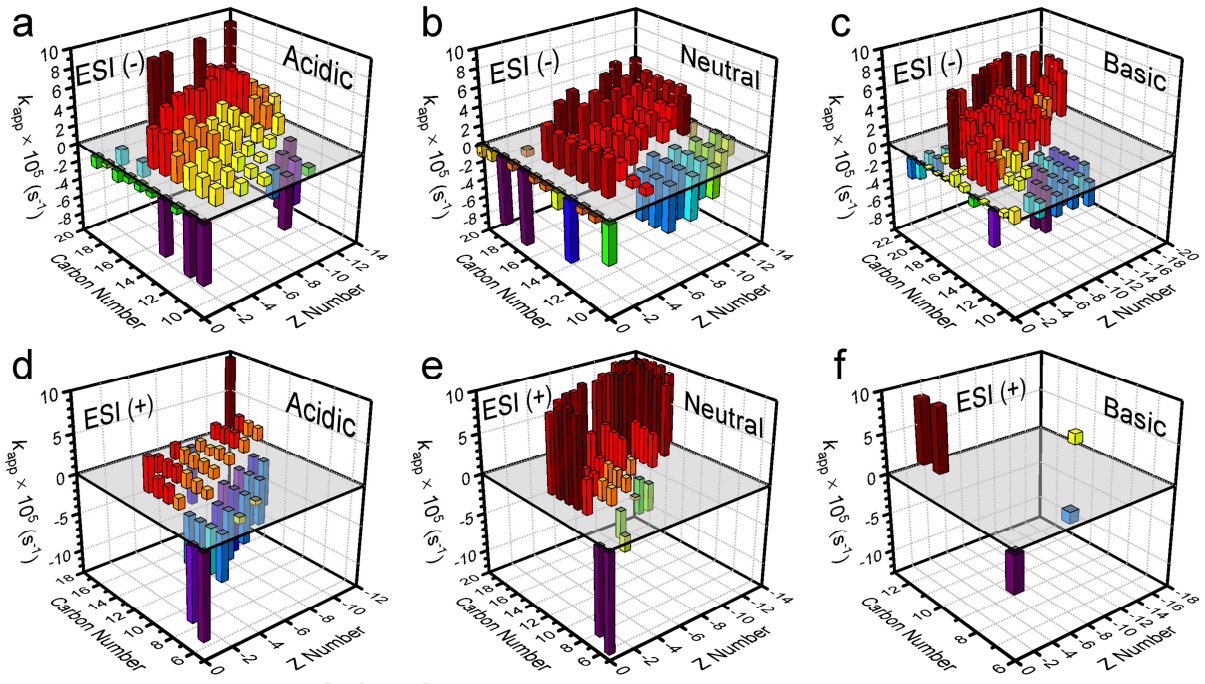

405

406 **Figure 5.** Estimates of pseudo-first order rate constants (k_{app}) of photocatalytic degradation of
407 (a)-(c) O_2^- and (d)-(f) O_2^+ species in the (a)&(d) AEO, (b)&(e) NEO and (c)&(f) BEO fractions.
408 Positive k_{app} values indicate rates of disappearance, while rates of appearance of new species
409 are plotted as negative values of k_{app}.

410 The initial raw OSPW profiles of $O_2^{\pm}$ in each of the extracts are presented in Figure S41. For the
411 O_2^-, the NEO and BEO were distributed to higher *c* and $|Z|$ relative to the AEO, which is as

412 expected, since only the most hydrophobic NAs (highest ratio of aliphatic carbon to the
413 carboxylate anion) should be extractable at higher pH values. In ESI(+), the O_2^+ distribution in
414 NEO was also shifted to slightly higher *c* and |*Z*| numbers versus the AEO.

415 The photocatalytic kinetics show a clear trend, across all fractions, of reactivity increasing with
416 carbon number (Figure 5), up to $k_{app} \approx 10 \times 10^{-5}$ s^{-1} for congeners of highest *c*. Furthermore, new
417 species of lower *c* and |*Z*| numbers, which did not appear in the initial profiles (Figure S41),
418 were produced over the course of the treatment (represented as negative values of k_{app} in
419 Figure 5). These smaller, more linear NOCs are likely generated from heavier, more cyclic
420 parent compounds through photocatalytic C-C bond scission, *e.g.*, via ring opening or
421 decarboxylative chain shortening. Indeed, it is likely that the true rate constants are
422 approximately equal across the O_2^- class and largely independent of *c* and *Z*, as would be
423 expected for a non-specific $HO^\bullet$ directed AOP. The apparent dependence may thus simply result
424 from intermediate *c* and |*Z*| numbered organics being simultaneously created from the
425 degradation of higher *c* and |*Z*| numbered species. Similarly, if acid-extractable O_2^+ compounds
426 are indeed hydroxylated aldehydes or ketones (Rowland et al., 2014; J. Sun et al., 2017), the
427 relatively lower rate constants in Figure 5d could be interpreted as evidence of their formation
428 during PC. Indeed, this would be expected from multiple pathways of $O_2^{\bullet-}$ driven C-C
429 cleavage.(Cermenati et al., 2000; Lair et al., 2008; Soana et al., 2000)

430 The environmental significance of these results is that both the most toxic and environmentally
431 persistent NAs are preferentially eliminated during PC treatment. Hughes et al. reported that
432 NAs with $c \geq 17$ were the most acutely toxic constituents of OSPW to rainbow trout
433 (*Oncorhynchus mykiss*).(Hughes et al., 2017b) Likewise, Yue et al. found that NAs with $14 \leq c \leq$

18 and -6 ≤ *Z* ≤ -4 were those most correlated with acute toxicity towards *Vibrio fischeri*,(Yue et al., 2015b) similar to the trend of increasing NA toxicity with *c* measured by Jones et al.(Jones et al., 2011) Similarly, NOCs with high *c* and |*Z*| numbers are known to be the most recalcitrant fractions in OSPW, while smaller and less cyclic NAs are more readily biodegradable.(Han et al., 2009, 2008; Holowenko et al., 2002) However, further research is merited to evaluate the toxicity of the lower *c* and |*Z*| numbered intermediates formed during the PC treatment process.

Conclusions

With recent insights into the structure-activity relationships driving various modes of observed OSPW toxicity, it is clear that specific classes of organics, comprising only a minority of the total NOCs, constitute the majority of the toxicity associated with OSPW.(Hughes et al., 2017b; Morandi et al., 2015) Through implementing a fractionated HRMS investigation, these NOCOCs could be individually tracked in the context of PC oxidation trends occurring in the NOCs as a whole. Revelation that the OS^+ and NO^+ classes were eliminated in the earliest stages of the PC reaction, and that the highest molecular weight O_2^- NAs were preferentially degraded, may indicate that only relatively low solar doses would be required to detoxify OSPW. This could result in more efficient treatments as compared to the solar exposures required for complete NOCs oxidation or DOC mineralization. This study also demonstrates application of a buoyant photocatalyst formulation as a passive treatment concept for oil sands remediation challenges. Further studies to develop this paradigm of a passive AOP are ongoing in our lab.

Acknowledgements

We thank the industrial producer that supplied OSPW samples for our experiments. We wish to thank Prof. Tong Leung and Marwa Abd-Ellah, Department of Chemistry, University of Waterloo, for assistance with the SEM analysis. We also thank John Tse for assistance with the BPC recyclability study. This work was financially supported by the Natural Sciences and Engineering Research Council of Canada, and Tim Leshuk gratefully acknowledges support of the NSERC Vanier Canada Graduate Scholarship and Ontario Graduate Scholarship.

Conflict of Interest

The following authors, T.L. and F.G., declare involvement as co-founders (with stock ownership) in H2nanO Inc., an organization with a financial interest in the subject matter and materials discussed in this manuscript. The following authors, K.M.P, D.d.O.L., A.T., P.B., and J.V.H. declare no competing financial interest.

References

Alharbi, H.A., Saunders, D.M.V., Al-Mousa, A., Alcorn, J., Pereira, A.S., Martin, J.W., Giesy, J.P., Wiseman, S.B., 2016. Inhibition of ABC transport proteins by oil sands process affected water. Aquat. Toxicol. 170, 81–88. https://doi.org/10.1016/j.aquatox.2015.11.013

Allain, E., Besson, S., Durand, C., Moreau, M., Gacoin, T., Boilot, J.-P., 2007. Transparent Mesoporous Nanocomposite Films for Self-Cleaning Applications. Adv. Funct. Mater. 17, 549–554. https://doi.org/10.1002/adfm.200600197

Araña, J., Garriga i Cabo, C., Fernández Rodríguez, C., Herrera Melián, J.A., Ortega Méndez, J.A., Doña Rodríguez, J.M., Pérez Peña, J., 2008. Combining TiO2-photocatalysis and wetland reactors for the efficient treatment of pesticides. Chemosphere 71, 788–794. https://doi.org/10.1016/j.chemosphere.2007.10.008

Barrow, M.P., Peru, K.M., Fahlman, B., Hewitt, L.M., Frank, R.A., Headley, J.V., 2015. Beyond Naphthenic Acids: Environmental Screening of Water from Natural Sources and the Athabasca Oil Sands Industry Using Atmospheric Pressure Photoionization Fourier Transform Ion Cyclotron Resonance Mass Spectrometry. J. Am. Soc. Mass Spectrom. 1–14. https://doi.org/10.1007/s13361-015-1188-9

Barrow, M.P., Peru, K.M., Headley, J.V., 2014. An Added Dimension: GC Atmospheric Pressure Chemical Ionization FTICR MS and the Athabasca Oil Sands. Anal. Chem. 86, 8281–8288. https://doi.org/10.1021/ac501710y

Barrow, M.P., Peru, K.M., McMartin, D.W., Headley, J.V., 2016. Effects of Extraction pH on the Fourier Transform Ion Cyclotron Resonance Mass Spectrometry Profiles of Athabasca Oil Sands Process Water. Energy Fuels 30, 3615–3621. https://doi.org/10.1021/acs.energyfuels.5b02086

Barrow, M.P., Witt, M., Headley, J.V., Peru, K.M., 2010. Athabasca Oil Sands Process Water: Characterization by Atmospheric Pressure Photoionization and Electrospray Ionization Fourier Transform Ion Cyclotron Resonance Mass Spectrometry. Anal. Chem. 82, 3727–3735. https://doi.org/10.1021/ac100103y

Berry, R.J., Mueller, M.R., 1994. Photocatalytic Decomposition of Crude Oil Slicks Using TiO2 on a Floating Substrate. Microchem. J. 50, 28–32. https://doi.org/10.1006/mchj.1994.1054

Brown, L.D., Pérez-Estrada, L., Wang, N., El-Din, M.G., Martin, J.W., Fedorak, P.M., Ulrich, A.C., 2013. Indigenous microbes survive in situ ozonation improving biodegradation of dissolved organic matter in aged oil sands process-affected waters. Chemosphere 93, 2748–2755. https://doi.org/10.1016/j.chemosphere.2013.09.026

Brown, L.D., Ulrich, A.C., 2015. Oil sands naphthenic acids: A review of properties, measurement, and treatment. Chemosphere 127, 276–290. https://doi.org/10.1016/j.chemosphere.2015.02.003

Bui, T.D., Kimura, A., Higashida, S., Ikeda, S., Matsumura, M., 2011. Two routes for mineralizing benzene by TiO2-photocatalyzed reaction. Appl. Catal., B 107, 119–127. https://doi.org/10.1016/j.apcatb.2011.07.004

Cermenati, L., Albini, A., Pichat, P., Guillard, C., 2000. TiO2 photocatalytic degradation of haloquinolines in water: Aromatic products GM-MS identification. Role of electron

509 transfer and superoxide. Res. Chem. Intermed. 26, 221–234.
510 https://doi.org/10.1163/156856700X00741
511 Chong, M.N., Jin, B., Chow, C.W.K., Saint, C., 2010. Recent developments in photocatalytic
512 water treatment technology: A review. Water Res. 44, 2997–3027.
513 https://doi.org/10.1016/j.watres.2010.02.039
514 Chow, K.L., Man, Y.B., Tam, N.F.Y., Liang, Y., Wong, M.H., 2017. Removal of decabromodiphenyl
515 ether (BDE-209) using a combined system involving TiO2 photocatalysis and wetland
516 plants. J. Hazard. Mater., SI:Environmental Nanotechnol 322, 263–269.
517 https://doi.org/10.1016/j.jhazmat.2016.05.097
518 Clemente, J.S., Fedorak, P.M., 2005. A review of the occurrence, analyses, toxicity, and
519 biodegradation of naphthenic acids. Chemosphere 60, 585–600.
520 https://doi.org/10.1016/j.chemosphere.2005.02.065
521 COSIA Challenge #0014: Passive Organics Treatment Technology [WWW Document], 2015. .
522 COSIA's Water Challenges. URL http://www.cosia.ca/initiatives/water/water-challenge-
523 statements (accessed 10.29.16).
524 Damasceno, F.C., Gruber, L.D.A., Geller, A.M., Campos, M.C.V. de, Gomes, A.O., Guimarães,
525 R.C.L., Péres, V.F., Jacques, R.A., Caramão, E.B., 2014. Characterization of naphthenic
526 acids using mass spectroscopy and chromatographic techniques: study of technical
527 mixtures. Anal. Methods 6, 807–816. https://doi.org/10.1039/C3AY40851E
528 D'Auria, M., Emanuele, L., Racioppi, R., Velluzzi, V., 2009. Photochemical degradation of crude
529 oil: Comparison between direct irradiation, photocatalysis, and photocatalysis on
530 zeolite. Journal of Hazardous Materials 164, 32–38.
531 https://doi.org/10.1016/j.jhazmat.2008.07.111
532 de Oliveira Livera, D., Leshuk, T., Peru, K.M., Headley, J.V., Gu, F., 2018. Structure-reactivity
533 relationship of naphthenic acids in the photocatalytic degradation process.
534 Chemosphere 200, 180–190. https://doi.org/10.1016/j.chemosphere.2018.02.049
535 Directive 085: Fluid Tailings Management for Oil Sands Mining Projects, 2017. . Alberta Energy
536 Regulator.
537 Dobson, K.D., McQuillan, A.J., 1999. In situ infrared spectroscopic analysis of the adsorption of
538 aliphatic carboxylic acids to TiO2, ZrO2, Al2O3, and Ta2O5 from aqueous solutions.
539 Spectrochim. Acta, A. 55, 1395–1405. https://doi.org/10.1016/S1386-1425(98)00303-5
540 Dong, T., Zhang, Y., Islam, M.S., Liu, Y., Gamal El-Din, M., 2015. The impact of various ozone
541 pretreatment doses on the performance of endogenous microbial communities for the
542 remediation of oil sands process-affected water. Int. Biodeterior. Biodegrad. 100, 17–28.
543 https://doi.org/10.1016/j.ibiod.2015.01.014
544 Fabiyi, M.E., Skelton, R.L., 2000. Photocatalytic mineralisation of methylene blue using buoyant
545 TiO2-coated polystyrene beads. J. Photochem. Photobiol., A 132, 121–128.
546 https://doi.org/10.1016/S1010-6030(99)00250-6
547 Frank, R.A., Fischer, K., Kavanagh, R., Burnison, B.K., Arsenault, G., Headley, J.V., Peru, K.M.,
548 Kraak, G.V.D., Solomon, K.R., 2009. Effect of Carboxylic Acid Content on the Acute
549 Toxicity of Oil Sands Naphthenic Acids. Environ. Sci. Technol. 43, 266–271.
550 https://doi.org/10.1021/es8021057
551 Frank, R.A., Kavanagh, R., Kent Burnison, B., Arsenault, G., Headley, J.V., Peru, K.M., Van Der
552 Kraak, G., Solomon, K.R., 2008. Toxicity assessment of collected fractions from an

553 extracted naphthenic acid mixture. Chemosphere 72, 1309–1314.
554 https://doi.org/10.1016/j.chemosphere.2008.04.078
555 Frank, R.A., Roy, J.W., Bickerton, G., Rowland, S.J., Headley, J.V., Scarlett, A.G., West, C.E., Peru,
556 K.M., Parrott, J.L., Conly, F.M., Hewitt, L.M., 2014. Profiling Oil Sands Mixtures from
557 Industrial Developments and Natural Groundwaters for Source Identification. Environ.
558 Sci. Technol. 48, 2660–2670. https://doi.org/10.1021/es500131k
559 Froggett, S.J., Clancy, S.F., Boverhof, D.R., Canady, R.A., 2014. A review and perspective of
560 existing research on the release of nanomaterials from solid nanocomposites. Particle
561 Fibre Toxicol. 11, 17. https://doi.org/10.1186/1743-8977-11-17
562 García-Martínez, M.J., Da Riva, I., Canoira, L., Llamas, J.F., Alcántara, R., Gallego, J.L.R., 2006.
563 Photodegradation of polycyclic aromatic hydrocarbons in fossil fuels catalysed by
564 supported TiO2. Applied Catalysis B: Environmental 67, 279–289.
565 https://doi.org/10.1016/j.apcatb.2006.05.013
566 Ging, J., Tejerina-Anton, R., Ramakrishnan, G., Nielsen, M., Murphy, K., Gorham, J.M., Nguyen,
567 T., Orlov, A., 2014. Development of a conceptual framework for evaluation of
568 nanomaterials release from nanocomposites: Environmental and toxicological
569 implications. Sci. Total Environ. 473–474, 9–19.
570 https://doi.org/10.1016/j.scitotenv.2013.11.135
571 Grabowska, E., Reszczyńska, J., Zaleska, A., 2012. Mechanism of phenol photodegradation in
572 the presence of pure and modified-TiO2: A review. Water Res. 46, 5453–5471.
573 https://doi.org/10.1016/j.watres.2012.07.048
574 Grewer, D.M., Young, R.F., Whittal, R.M., Fedorak, P.M., 2010. Naphthenic acids and other acid-
575 extractables in water samples from Alberta: What is being measured? Sci. Total Environ.
576 408, 5997–6010. https://doi.org/10.1016/j.scitotenv.2010.08.013
577 Griffiths, M.T., Da Campo, R., O'Connor, P.B., Barrow, M.P., 2014. Throwing Light on Petroleum:
578 Simulated Exposure of Crude Oil to Sunlight and Characterization Using Atmospheric
579 Pressure Photoionization Fourier Transform Ion Cyclotron Resonance Mass
580 Spectrometry. Anal. Chem. 86, 527–534. https://doi.org/10.1021/ac4025335
581 Han, X., MacKinnon, M.D., Martin, J.W., 2009. Estimating the in situ biodegradation of
582 naphthenic acids in oil sands process waters by HPLC/HRMS. Chemosphere 76, 63–70.
583 https://doi.org/10.1016/j.chemosphere.2009.02.026
584 Han, X., Scott, A.C., Fedorak, P.M., Bataineh, M., Martin, J.W., 2008. Influence of Molecular
585 Structure on the Biodegradability of Naphthenic Acids. Environ. Sci. Technol. 42, 1290–
586 1295. https://doi.org/10.1021/es702220c
587 Headley, J.V., Barrow, M.P., Peru, K.M., Fahlman, B., Frank, R.A., Bickerton, G., McMaster, M.E.,
588 Parrott, J., Hewitt, L.M., 2011. Preliminary fingerprinting of Athabasca oil sands polar
589 organics in environmental samples using electrospray ionization Fourier transform ion
590 cyclotron resonance mass spectrometry. Rapid Commun. Mass Spectrom. 25, 1899–
591 1909. https://doi.org/10.1002/rcm.5062
592 Headley, J.V., Du, J.-L., Peru, K.M., McMartin, D.W., 2009. Electrospray ionization mass
593 spectrometry of the photodegradation of naphthenic acids mixtures irradiated with
594 titanium dioxide. J. Environ. Sci. Health, Part A 44, 591–597.
595 https://doi.org/10.1080/10934520902784625

596 Headley, J.V., Peru, K.M., Mohamed, M.H., Frank, R.A., Martin, J.W., Hazewinkel, R.R.O.,
597 Humphries, D., Gurprasad, N.P., Hewitt, L.M., Muir, D.C.G., Lindeman, D., Strub, R.,
598 Young, R.F., Grewer, D.M., Whittal, R.M., Fedorak, P.M., Birkholz, D.A., Hindle, R.,
599 Reisdorph, R., Wang, X., Kasperski, K.L., Hamilton, C., Woudneh, M., Wang, G., Loescher,
600 B., Farwell, A., Dixon, D.G., Ross, M., Pereira, A.D.S., King, E., Barrow, M.P., Fahlman, B.,
601 Bailey, J., Mcmartin, D.W., Borchers, C.H., Ryan, C.H., Toor, N.S., Gillis, H.M., Zuin, L.,
602 Bickerton, G., Mcmaster, M., Sverko, E., Shang, D., Wilson, L.D., Wrona, F.J., 2013.
603 Chemical fingerprinting of naphthenic acids and oil sands process waters—A review of
604 analytical methods for environmental samples. J. Environ. Sci. Health, Part A 48, 1145–
605 1163. https://doi.org/10.1080/10934529.2013.776332
606 Holowenko, F.M., MacKinnon, M.D., Fedorak, P.M., 2002. Characterization of naphthenic acids
607 in oil sands wastewaters by gas chromatography-mass spectrometry. Water Res. 36,
608 2843–2855. https://doi.org/10.1016/S0043-1354(01)00492-4
609 Holowenko, F.M., MacKinnon, M.D., Fedorak, P.M., 2001. Naphthenic acids and surrogate
610 naphthenic acids in methanogenic microcosms. Water Res. 35, 2595–2606.
611 https://doi.org/10.1016/S0043-1354(00)00558-3
612 Huang, R., McPhedran, K.N., Sun, N., Chelme-Ayala, P., Gamal El-Din, M., 2016. Investigation of
613 the impact of organic solvent type and solution pH on the extraction efficiency of
614 naphthenic acids from oil sands process-affected water. Chemosphere 146, 472–477.
615 https://doi.org/10.1016/j.chemosphere.2015.12.054
616 Hughes, S.A., Huang, R., Mahaffey, A., Chelme-Ayala, P., Klamerth, N., Meshref, M.N.A.,
617 Ibrahim, M.D., Brown, C., Peru, K.M., Headley, J.V., Gamal El-Din, M., 2017a.
618 Comparison of methods for determination of total oil sands-derived naphthenic acids in
619 water samples. Chemosphere 187, 376–384.
620 https://doi.org/10.1016/j.chemosphere.2017.08.123
621 Hughes, S.A., Mahaffey, A., Shore, B., Baker, J., Kilgour, B., Brown, C., Peru, K.M., Headley, J.V.,
622 Bailey, H.C., 2017b. Using ultrahigh-resolution mass spectrometry and toxicity
623 identification techniques to characterize the toxicity of oil sands process-affected water:
624 The case for classical naphthenic acids. Environ. Toxicol. Chem. 36, 3148–3157.
625 https://doi.org/10.1002/etc.3892
626 Islam, M.S., Moreira, J., Chelme-Ayala, P., Gamal El-Din, M., 2014. Prediction of naphthenic acid
627 species degradation by kinetic and surrogate models during the ozonation of oil sands
628 process-affected water. Sci. Total Environ. 493, 282–290.
629 https://doi.org/10.1016/j.scitotenv.2014.05.138
630 Janković, I.A., Šaponjić, Z.V., Čomor, M.I., Nedeljković, J.M., 2009. Surface Modification of
631 Colloidal TiO2 Nanoparticles with Bidentate Benzene Derivatives. J. Phys. Chem. C 113,
632 12645–12652. https://doi.org/10.1021/jp9013338
633 Jivraj, M.N., MacKinnon, M., Fung, B., 1995. Naphthenic Acid Extraction and Quantitative
634 Analysis with FT-IR Spectroscopy (Technical Report). Syncrude Canada Ltd., Edmonton,
635 Alberta.
636 Jones, D., Scarlett, A.G., West, C.E., Rowland, S.J., 2011. Toxicity of Individual Naphthenic Acids
637 to Vibrio fischeri. Environ. Sci. Technol. 45, 9776–9782.
638 https://doi.org/10.1021/es201948j

639 Klamerth, N., Moreira, J., Li, C., Singh, A., McPhedran, K.N., Chelme-Ayala, P., Belosevic, M.,
640 Gamal El-Din, M., 2015. Effect of ozonation on the naphthenic acids' speciation and
641 toxicity of pH-dependent organic extracts of oil sands process-affected water. Sci. Total
642 Environ. 506–507, 66–75. https://doi.org/10.1016/j.scitotenv.2014.10.103
643 Lair, A., Ferronato, C., Chovelon, J.-M., Herrmann, J.-M., 2008. Naphthalene degradation in
644 water by heterogeneous photocatalysis: An investigation of the influence of inorganic
645 anions. J. Photochem. Photobiol., A 193, 193–203.
646 https://doi.org/10.1016/j.jphotochem.2007.06.025
647 Leshuk, T., de Oliveira Livera, D., Peru, K.M., Headley, J.V., Vijayaraghavan, S., Wong, T., Gu, F.,
648 2016a. Photocatalytic degradation kinetics of naphthenic acids in oil sands process-
649 affected water: Multifactorial determination of significant factors. Chemosphere 165,
650 10–17. https://doi.org/10.1016/j.chemosphere.2016.08.115
651 Leshuk, T., Wong, T., Linley, S., Peru, K.M., Headley, J.V., Gu, F., 2016b. Solar photocatalytic
652 degradation of naphthenic acids in oil sands process-affected water. Chemosphere 144,
653 1854–1861. https://doi.org/10.1016/j.chemosphere.2015.10.073
654 Liu, J., Wang, L., Tang, J., Ma, J., 2016. Photocatalytic degradation of commercially sourced
655 naphthenic acids by TiO2-graphene composite nanomaterial. Chemosphere 149, 328–
656 335. https://doi.org/10.1016/j.chemosphere.2016.01.074
657 Lower Athabasca Region - Tailings Management Framework for the Mineable Athabasca Oil
658 Sands, 2015. . Government of Alberta.
659 Magalhães, F., Lago, R.M., 2009. Floating photocatalysts based on TiO2 grafted on expanded
660 polystyrene beads for the solar degradation of dyes. Sol. Energy 83, 1521–1526.
661 https://doi.org/10.1016/j.solener.2009.04.005
662 Malato, S., Fernandez-Ibanez, P., Maldonado, M., Blanco, J., Gernjak, W., 2009.
663 Decontamination and disinfection of water by solar photocatalysis: Recent overview and
664 trends. Catal. Today 147, 1–59. https://doi.org/10.1016/j.cattod.2009.06.018
665 Marentette, J.R., Frank, R.A., Bartlett, A.J., Gillis, P.L., Hewitt, L.M., Peru, K.M., Headley, J.V.,
666 Brunswick, P., Shang, D., Parrott, J.L., 2015. Toxicity of naphthenic acid fraction
667 components extracted from fresh and aged oil sands process-affected waters, and
668 commercial naphthenic acid mixtures, to fathead minnow (Pimephales promelas)
669 embryos. Aquat. Toxicol. 164, 108–117. https://doi.org/10.1016/j.aquatox.2015.04.024
670 Marshall, A.G., Rodgers, R.P., 2008. Petroleomics: Chemistry of the underworld. Proc. Natl.
671 Acad. Sci. U.S.A. 105, 18090–18095. https://doi.org/10.1073/pnas.0805069105
672 Martin, J.W., 2015. The Challenge: Safe release and reintegration of oil sands process-affected
673 water. Environ. Toxicol. Chem. 34, 2682–2682. https://doi.org/10.1002/etc.3139
674 Martin, J.W., Barri, T., Han, X., Fedorak, P.M., El-Din, M.G., Perez, L., Scott, A.C., Jiang, J.T., 2010.
675 Ozonation of Oil Sands Process-Affected Water Accelerates Microbial Bioremediation.
676 Environ. Sci. Technol. 44, 8350–8356. https://doi.org/10.1021/es101556z
677 McKenna, A.M., Nelson, R.K., Reddy, C.M., Savory, J.J., Kaiser, N.K., Fitzsimmons, J.E., Marshall,
678 A.G., Rodgers, R.P., 2013. Expansion of the Analytical Window for Oil Spill
679 Characterization by Ultrahigh Resolution Mass Spectrometry: Beyond Gas
680 Chromatography. Environ. Sci. Technol. 47, 7530–7539.
681 https://doi.org/10.1021/es305284t

McQueen, A.D., Hendrikse, M., Gaspari, D.P., Kinley, C.M., Rodgers Jr., J.H., Castle, J.W., 2017a. Performance of a hybrid pilot-scale constructed wetland system for treating oil sands process-affected water from the Athabasca oil sands. Ecol. Eng. 102, 152–165. https://doi.org/10.1016/j.ecoleng.2017.01.024

McQueen, A.D., Kinley, C.M., Hendrikse, M., Gaspari, D.P., Calomeni, A.J., Iwinski, K.J., Castle, J.W., Haakensen, M.C., Peru, K.M., Headley, J.V., Rodgers Jr., J.H., 2017b. A risk-based approach for identifying constituents of concern in oil sands process-affected water from the Athabasca Oil Sands region. Chemosphere 173, 340–350. https://doi.org/10.1016/j.chemosphere.2017.01.072

Meshref, M.N.A., Chelme-Ayala, P., Gamal El-Din, M., 2017. Fate and abundance of classical and heteroatomic naphthenic acid species after advanced oxidation processes: Insights and indicators of transformation and degradation. Water Research 125, 62–71. https://doi.org/10.1016/j.watres.2017.08.007

Mishra, S., Meda, V., Dalai, A.K., McMartin, D.W., Headley, J.V., Peru, K.M., 2010. Photocatalysis of Naphthenic Acids in Water. J. Water Resour. Prot. 02, 644–650. https://doi.org/10.4236/jwarp.2010.27074

Mohamed, M.H., Wilson, L.D., Headley, J.V., Peru, K.M., 2008. Screening of oil sands naphthenic acids by UV-Vis absorption and fluorescence emission spectrophotometry. J. Environ. Sci. Health, Part A 43, 1700–1705. https://doi.org/10.1080/10934520802330255

Morandi, G.D., Wiseman, S.B., Guan, M., Zhang, X.W., Martin, J.W., Giesy, J.P., 2017. Elucidating mechanisms of toxic action of dissolved organic chemicals in oil sands process-affected water (OSPW). Chemosphere 186, 893–900. https://doi.org/10.1016/j.chemosphere.2017.08.025

Morandi, G.D., Wiseman, S.B., Pereira, A., Mankidy, R., Gault, I.G.M., Martin, J.W., Giesy, J.P., 2015. Effects-Directed Analysis of Dissolved Organic Compounds in Oil Sands Process-Affected Water. Environ. Sci. Technol. 49, 12395–12404. https://doi.org/10.1021/acs.est.5b02586

Morandi, G.D., Zhang, K., Wiseman, S.B., Pereira, A. dos S., Martin, J.W., Giesy, J.P., 2016. Effect of Lipid Partitioning on Predictions of Acute Toxicity of Oil Sands Process Affected Water to Embryos of Fathead Minnow (Pimephales promelas). Environ. Sci. Technol. 50, 8858–8866. https://doi.org/10.1021/acs.est.6b01481

Nair, M., Luo, Z., Heller, A., 1993. Rates of photocatalytic oxidation of crude oil on salt water on buoyant, cenosphere-attached titanium dioxide. Ind. Eng. Chem. Res. 32, 2318–2323. https://doi.org/10.1021/ie00022a015

Nosaka, Y., Nosaka, A.Y., 2013. Identification and Roles of the Active Species Generated on Various Photocatalysts, in: Pichat, P. (Ed.), Photocatalysis and Water Purification. Wiley-VCH Verlag GmbH & Co. KGaA, pp. 1–24.

Payne, J.R., Phillips, C.R., 1985. Photochemistry of petroleum in water. Environ. Sci. Technol. 19, 569–579. https://doi.org/10.1021/es00137a602

Pereira, A.S., Bhattacharjee, S., Martin, J.W., 2013. Characterization of Oil Sands Process-Affected Waters by Liquid Chromatography Orbitrap Mass Spectrometry. Environ. Sci. Technol. 47, 5504–5513. https://doi.org/10.1021/es401335t

Pichat, P., 1997. Photocatalytic degradation of aromatic and alicyclic pollutants in water: by-products, pathways and mechanisms. Water Sci. Technol., Oxidation Technologies for

726 Water and Wastewater Treatment Selected Proceedings of the International Conference
727 on Oxidation Technologies for Water and Wastewater Treatment 35, 73–78.
728 https://doi.org/10.1016/S0273-1223(97)00011-5
729 Qiu, W., Zheng, Y., 2007. A comprehensive assessment of supported titania photocatalysts in a
730 fluidized bed photoreactor: Photocatalytic activity and adherence stability. Appl. Catal. B
731 71, 151–162. https://doi.org/10.1016/j.apcatb.2006.08.021
732 Quagraine, E.K., Peterson, H.G., Headley, J.V., 2005. In Situ Bioremediation of Naphthenic Acids
733 Contaminated Tailing Pond Waters in the Athabasca Oil Sands Region—Demonstrated
734 Field Studies and Plausible Options: A Review. J. Environ. Sci. Health, Part A 40, 685–722.
735 https://doi.org/10.1081/ESE-200046649
736 Quesnel, D.M., Oldenburg, T.B.P., Larter, S.R., Gieg, L.M., Chua, G., 2015. Biostimulation of Oil
737 Sands Process-Affected Water with Phosphate Yields Removal of Sulfur-Containing
738 Organics and Detoxification. Environ. Sci. Technol. 49, 13012–13020.
739 https://doi.org/10.1021/acs.est.5b01391
740 Roberts, D.W., Costello, J.F., 2003. Mechanisms of action for general and polar narcosis: A
741 difference in dimension. QSAR Comb. Sci. 22, 226–233.
742 https://doi.org/10.1002/qsar.200390016
743 Rowland, S.J., Pereira, A.S., Martin, J.W., Scarlett, A.G., West, C.E., Lengger, S.K., Wilde, M.J.,
744 Pureveen, J., Tegelaar, E.W., Frank, R.A., Hewitt, L.M., 2014. Mass spectral
745 characterisation of a polar, esterified fraction of an organic extract of an oil sands
746 process water. Rapid Commun. Mass Spectrom. 28, 2352–2362.
747 https://doi.org/10.1002/rcm.7024
748 Rowland, S.J., West, C.E., Jones, D., Scarlett, A.G., Frank, R.A., Hewitt, L.M., 2011. Steroidal
749 Aromatic 'Naphthenic Acids' in Oil Sands Process-Affected Water: Structural
750 Comparisons with Environmental Estrogens. Environ. Sci. Technol. 45, 9806–9815.
751 https://doi.org/10.1021/es202606d
752 Scott, A.C., Zubot, W., MacKinnon, M.D., Smith, D.W., Fedorak, P.M., 2008. Ozonation of oil
753 sands process water removes naphthenic acids and toxicity. Chemosphere 71, 156–160.
754 https://doi.org/10.1016/j.chemosphere.2007.10.051
755 Shang, J., Chai, M., Zhu, Y., 2003. Photocatalytic degradation of polystyrene plastic under
756 fluorescent light. Environ. Sci. Technol. 37, 4494–4499.
757 Shankar, R., Shim, W.J., An, J.G., Yim, U.H., 2015. A practical review on photooxidation of crude
758 oil: Laboratory lamp setup and factors affecting it. Water Research 68, 304–315.
759 https://doi.org/10.1016/j.watres.2014.10.012
760 Singh, S., Mahalingam, H., Singh, P.K., 2013. Polymer-supported titanium dioxide photocatalysts
761 for environmental remediation: A review. Appl. Catal. A 462–463, 178–195.
762 https://doi.org/10.1016/j.apcata.2013.04.039
763 Soana, F., Sturini, M., Cermenati, L., Albini, A., 2000. Titanium dioxide photocatalyzed
764 oxygenation of naphthalene and some of its derivatives. J. Chem. Soc., Perkin Trans. 2
765 699–704. https://doi.org/10.1039/A908945D
766 Sun, C., Shotyk, W., Cuss, C.W., Donner, M.W., Fennell, J., Javed, M., Noernberg, T., Poesch, M.,
767 Pelletier, R., Sinnatamby, N., Siddique, T., Martin, J.W., 2017. Characterization of
768 Naphthenic Acids and Other Dissolved Organics in Natural Water from the Athabasca Oil

769 Sands Region, Canada. Environ. Sci. Technol. 51, 9524–9532.
770 https://doi.org/10.1021/acs.est.7b02082
771 Sun, J., Peng, H., Alharbi, H.A., Jones, P.D., Giesy, J.P., Wiseman, S.B., 2017. Identification of
772 Chemicals that Cause Oxidative Stress in Oil Sands Process-Affected Water. Environ. Sci.
773 Technol. 51, 8773–8781. https://doi.org/10.1021/acs.est.7b01987
774 Verbeek, A.G., Mackay, W.C., MacKinnon, M.D., 1994. Acute toxicity of oil sands wastewater: A
775 toxic balance, in: Proceedings of the Twentieth Annual Aquatic Toxicity Workshop. p. 9.
776 Wang, C., Huang, R., Klamerth, N., Chelme-Ayala, P., Gamal El-Din, M., 2016. Positive and
777 negative electrospray ionization analyses of the organic fractions in raw and oxidized oil
778 sands process-affected water. Chemosphere 165, 239–247.
779 https://doi.org/10.1016/j.chemosphere.2016.09.009
780 Yue, S., Ramsay, B.A., Brown, R.S., Wang, J., Ramsay, J.A., 2015a. Identification of Estrogenic
781 Compounds in Oil Sands Process Waters by Effect Directed Analysis. Environ. Sci.
782 Technol. 49, 570–577. https://doi.org/10.1021/es5039134
783 Yue, S., Ramsay, B.A., Wang, J., Ramsay, J., 2015b. Toxicity and composition profiles of solid
784 phase extracts of oil sands process-affected water. Sci. Total Environ. 538, 573–582.
785 https://doi.org/10.1016/j.scitotenv.2015.08.079
786 Zhang, K., Pereira, A.S., Martin, J.W., 2015. Estimates of Octanol–Water Partitioning for
787 Thousands of Dissolved Organic Species in Oil Sands Process-Affected Water. Environ.
788 Sci. Technol. 49, 8907–8913. https://doi.org/10.1021/acs.est.5b01656
789 Zhang, K., Wiseman, S., Giesy, J.P., Martin, J.W., 2016. Bioconcentration of Dissolved Organic
790 Compounds from Oil Sands Process-Affected Water by Medaka (Oryzias latipes):
791 Importance of Partitioning to Phospholipids. Environ. Sci. Technol. 50, 6574–6582.
792 https://doi.org/10.1021/acs.est.6b01354
793 Ziolli, R.L., Jardim, W.F., 2003. Photochemical transformations of water-soluble fraction (WSF)
794 of crude oil in marine waters: A comparison between photolysis and accelerated
795 degradation with TiO2 using GC–MS and UVF. Journal of Photochemistry and
796 Photobiology A: Chemistry 155, 243–252. https://doi.org/10.1016/S1010-
797 6030(02)00397-0
798

799

Highlights

- Oil sands process-affected water (OSPW) is impacted by naphthenic organic compounds (NOCs)
- Majority of OSPW toxicity attributed to only a subset of NOC classes
- Passive treatment of OSPW demonstrated with buoyant photocatalyts
- First time petroleomics used to study treatment kinetics across NOC fractions
- Preferential degradation of priority O_2^-, OS^+ and NO^+ NOC classes of concern